*Korean J. Chem. Eng.*, **27**(4), 1123-1131 (2010)
DOI: 10.1007/s11814-010-0210-y

# Water-gas shift reaction over supported Pt and Pt-$CeO_x$ catalysts

**Yong Tae Kim and Eun Duck Park†**

Division of Energy Systems Research and Division of Chemical Engineering and Materials Engineering, Ajou University, Wonchun-dong, Yeongtong-gu, Suwon 443-749, Korea
(*Received 22 January 2010 • accepted 2 March 2010*)

**Abstract**−A comparison study was performed of the water-gas shift (WGS) reaction over Pt and ceria-promoted Pt catalysts supported on $CeO_2$, $ZrO_2$, and $TiO_2$ under rather severe reaction conditions: 6.7 mol% CO, 6.7 mol% $CO_2$, and 33.2 mol% $H_2O$ in $H_2$. Several techniques--CO chemisorption, temperature-programmed reduction (TPR), and inductively coupled plasma-atomic emission spectroscopy (ICP-AES)--were employed to characterize the catalysts. The WGS reaction rate increased with increasing amount of chemisorbed CO over Pt/$ZrO_2$, Pt/$TiO_2$, and Pt-$CeO_x$/$ZrO_2$, whereas no such correlation was found over Pt/$CeO_2$, Pt-$CeO_x$/$CeO_2$, and Pt-$CeO_x$/$TiO_2$. For these catalysts in the absence of any impurities such as $Na^+$, the WGS activity increased with increasing surface area of the support, showed a maximum value, and then decreased as the surface area of the support was further increased. An adverse effect of $Na^+$ on the amount of chemisorbed CO and the WGS activity was observed over Pt/$CeO_2$. Pt-$CeO_x$/$TiO_2$ (51) showed the highest WGS activity among the tested supported Pt and Pt-$CeO_x$ catalysts. The close contact between Pt and the support or between Pt and $CeO_x$, as monitored by $H_2$-TPR, is closely related to the WGS activity. The catalytic stability at 583 K improved with increasing surface area of the support over the $CeO_2$- and $ZrO_2$-supported Pt and Pt-$CeO_x$ catalysts.

Key words: Water-gas Shift, Pt, Ceria, Support, Fuel Cell

## INTRODUCTION

More attention has recently been paid to fuel cells due to the increasing need for highly efficient energy conversion systems. Since the present fuel cells, utilizing hydrogen as a fuel, require hydrocarbons as a raw fuel, it is desirable to develop highly efficient fuel processors in which hydrocarbons can be transformed into hydrogen through catalytic reactions such as the reforming and water-gas shift (WGS) reaction. The WGS reaction can decrease the CO concentration and increase the $H_2$ concentration simultaneously as follows.

$$CO(g)+H_2O(g)\leftrightarrow CO_2(g)+H_2(g),\ \Delta H^o_{298}=-41{,}166\ J/mol$$

Because this WGS reaction is exothermic and thermodynamically limited, it is conventionally carried out in a commercial $H_2$ plant via two-stage processes involving a high-temperature shifter (HTS~673 K) and a low-temperature shifter (LTS, around 473 K) [1]. Fe-based [2] and Cu-based [3] catalyst systems have been successfully implemented for these two processes, respectively. However, these catalyst systems suffer from certain drawbacks when used in small-scale fuel processors with characteristics such as cyclic operation and the possibility of air contamination [3,4]. To overcome these weak points of commercial WGS catalysts, some noble metal catalysts including Pt group metals have been extensively studied [5-22]. Panagiotopoulou and Kondarides [5] compared the WGS activity among various noble metal catalysts supported on $Al_2O_3$ and reported that the catalytic activity followed the order of Pt>Rh≈Ru>Pd. WGS activity in the order of Pt>Rh>Ru~Pd>Ir>Au was also revealed over noble metal catalysts supported on ceria-zirconia [12]. In the case of supported Pt and Ru catalysts, a higher turnover frequency was found when they were supported on reducible ($TiO_2$, $CeO_2$, $La_2O_3$, and YSZ) rather than on irreducible ($Al_2O_3$, MgO, and $SiO_2$) metal oxides [5].

Until now, the WGS performance has been measured over Pt-based catalysts supported on various supports such as $CeO_2$ [6-8, 14,15], $ZrO_2$ [9], $CeZrO_x$ [10-12], $TiZrO_x$ [13], and $TiO_2$ [16-22]. Recently, ceria-promoted Pt/$TiO_2$ catalysts have been reported to show quite promising WGS activity [20,22].

In our previous works [11,20], we found that the ceria-promoted Pt catalysts prepared using a single step co-impregnation method were more active for the WGS reaction than those prepared using a sequential impregnation method. Although some comparative studies of supported Pt catalysts have been reported, the effect of the surface area of the supports on the WGS activity has not been investigated in detail over supported Pt and Pt-$CeO_x$ catalysts.

In this work, we examined the effect of the surface area of the support on the WGS activity over Pt and Pt-$CeO_x$ catalysts supported on reducible metal oxides such as $CeO_2$, $ZrO_2$ and $TiO_2$. The catalytic stability was also investigated under severe reaction conditions.

## EXPERIMENTAL

### 1. Catalyst Preparation

Various supports, such as $CeO_2$ (Kanto Chemical Co., $S_{BET}$=8.9 $m^2/g$), $CeO_2$ (Rhodia, $S_{BET}$=300.0 $m^2/g$), $ZrO_2$ (Junsei Chemical Co., $S_{BET}$=2.3 $m^2/g$), $TiO_2$ (Junsei Chemical Co., $S_{BET}$=1.0 $m^2/g$), $TiO_2$ (Degussa, $S_{BET}$=51.3 $m^2/g$) and $TiO_2$ (Hombicat, $S_{BET}$=337.0 $m^2/g$), were purchased and used as received. Additionally, $CeO_2$ ($S_{BET}$=54.1

†To whom correspondence should be addressed.
E-mail: edpark@ajou.ac.kr

$m^2/g$), $ZrO_2$ ($S_{BET}$=75.0 $m^2/g$), and $TiO_2$ ($S_{BET}$=80.0 $m^2/g$) were prepared from $Ce(NO_3)_3 \cdot 6H_2O$ (Junsei Chemical Co.), $ZrCl_2O \cdot 8H_2O$ (Junsei Chemical Co.), and $TiCl_4$ (Kanto Chemical Co.) by the precipitation method using ammonia solution as a precipitant, respectively. $CeO_2$ ($S_{BET}$=75.0 $m^2/g$) was also prepared from $Ce(NO_3)_3 \cdot 6H_2O$ (Junsei Chemical Co.) by the precipitation method using sodium hydroxide (NaOH) as a precipitant. The precipitate was dried at 393 K overnight and calcined in air at 773 K.

Supported Pt catalysts were prepared by the wet impregnation method from a support and an aqueous solution of $Pt(NH_3)_4(NO_3)_2$ (Aldrich). Supported ceria-promoted Pt catalysts were prepared by co-impregnation from a support and an aqueous solution of $Pt(NH_3)_4(NO_3)_2$ and $Ce(NO_3)_3 \cdot 6H_2O$ (Junsei Chemical Co.). The content of Pt was intended to be 1 wt% and the molar ratio between Ce and Pt was intended to be fixed at 5. All of the catalysts were calcined in air at 773 K and reduced in a hydrogen stream at 673 K for 1 h before the reaction. To differentiate the catalysts, the specific surface area of the support used for each catalyst is presented in parentheses.

**2. Catalyst Characterization**

The chemical composition of the prepared samples was analyzed by inductively coupled plasma-atomic emission spectroscopy (ICP-AES, JY-70Plus, Jobin-Yvon), and the results are listed in Table 1.

The BET surface area was calculated based on the $N_2$ adsorption data obtained using an Autosorb-1 apparatus (Quantachrome) at liquid $N_2$ temperature. Before the measurement, the sample was degassed in a vacuum for 4 h at 473 K. The value for each catalyst is shown in Table 1.

The bulk crystalline structures of the catalysts were determined by the X-ray diffraction (XRD) technique. The XRD patterns were obtained with a Rigaku D/MAC-III using Cu K$\alpha$ radiation ($\lambda$=0.15406 nm), operated at 50 kV and 30 mA (1.5 kW). The assignment of the crystalline phases was carried out using PCPDFWIN software (version 2.2) with the ICDD database. The mole fraction of the tetragonal phase in $ZrO_2$ ($x_T$) [28] was estimated by the following equation:

$$x_T = \frac{I_{T(011)}}{1.6I_{M(\bar{1}11)} + I_{T(011)}} \times 100$$

where $I_{T(011)}$ and $I_{M(\bar{1}11)}$ represent the integral intensities of the tetragonal ($2\theta$=30.269°) and monoclinic ($2\theta$=28.175°) planes, respectively.

The mole fraction of the anatase phase in $TiO_2$ ($x_A$) [29] was also calculated by the following equation:

$$x_A = \frac{1}{1+1.26(I_{R(110)}/I_{A(101)})} \times 100$$

where $I_{R(110)}$ and $I_{A(101)}$ represents the integral intensities of the rutile ($2\theta$=27.446°) and anatase ($2\theta$=25.281°) planes, respectively.

The primary crystallite size of the support (L) was measured by Scherrer's equation.

$$L = \frac{0.9\lambda_{K\alpha 1}}{B_{(2\theta)}\cos\theta_{max}}$$

where L denotes the average particle size, 0.9 is a value when $B_{(2\theta)}$ is the full width at half maximum (FWHM) of the peak broadening in radians, $\lambda_{K\alpha 1}$ is the wavelength of the X-ray radiation (0.15406 nm), and $\theta_{max}$ is the angular position at the (111) peak maximum of $CeO_2$, the ($\bar{1}$11) peak maximum of $ZrO_2$, or the (101) peak maximum of $TiO_2$. Its value for each catalyst is presented in Table 2.

CO chemisorption was carried in an AutoChem 2910 unit (Micromeritics) equipped with a thermal conductivity detector (TCD) to measure the CO consumption and an on-line mass spectrometer (QMS 200, Pfeiffer Vacuum) to detect any organic or inorganic species in the effluent stream during CO chemisorption. Quartz U-tube

**Table 1. Physical properties of the supported Pt and Pt-$CeO_x$ catalysts**

| Catalysts | BET surface area ($m^2/g$) | Bulk composition (wt%)[a] | |
|---|---|---|---|
| | | Pt | Ce |
| $Pt/CeO_2$ (9) | 3.4 | 0.68 | 76.88 |
| $Pt/CeO_2$ (54) | 54.3 | 0.54 | 72.50 |
| $Pt/CeO_2$ (75) | 81.2 | 0.35 | 75.24 |
| $Pt/CeO_2$ (300) | 203.0 | 0.71 | 70.69 |
| $Pt/ZrO_2$ (2) | 4.1 | 0.53 | - |
| $Pt/ZrO_2$ (75) | 64.1 | 0.67 | - |
| $Pt/TiO_2$ (1) | 0.9 | 0.96 | - |
| $Pt/TiO_2$ (51) | 52.7 | 0.86 | - |
| $Pt/TiO_2$ (80) | 74.1 | 0.74 | - |
| $Pt/TiO_2$ (337) | 117.4 | 1.01 | - |
| $Pt\text{-}CeO_x/CeO_2$ (9) | 5.6 | 0.91 | 78.71 |
| $Pt\text{-}CeO_x/CeO_2$ (54) | 50.1 | 0.71 | 73.40 |
| $Pt\text{-}CeO_x/CeO_2$ (75) | 79.7 | 0.85 | 72.70 |
| $Pt\text{-}CeO_x/CeO_2$ (300) | 202.7 | 0.78 | 69.71 |
| $Pt\text{-}CeO_x/ZrO_2$ (2) | 9.4 | 0.75 | 2.79 |
| $Pt\text{-}CeO_x/ZrO_2$ (75) | 73.0 | 0.84 | 3.20 |
| $Pt\text{-}CeO_x/TiO_2$ (1) | 6.4 | 0.85 | 3.24 |
| $Pt\text{-}CeO_x/TiO_2$ (51) | 48.4 | 0.87 | 3.52 |
| $Pt\text{-}CeO_x/TiO_2$ (80) | 71.7 | 0.85 | 3.18 |
| $Pt\text{-}CeO_x/TiO_2$ (337) | 120.7 | 0.92 | 3.43 |

[a]The bulk composition was analyzed by ICP-AES

**Table 2. Physical properties of metal oxides**

| Support | Composition[a] (phase %) | The primary crystallite size[b] (nm) | BET surface area ($m^2/g$) |
|---|---|---|---|
| $CeO_2$ (9) | 100.0% | 44.8 | 8.9 |
| $CeO_2$ (54) | 100.0% | 13.4 | 54.1 |
| $CeO_2$ (75) | 100.0% | 9.6 | 75.0 |
| $CeO_2$ (300) | 100.0% | 4.8 | 300.0 |
| $ZrO_2$ (2) | 1.2% | 38.9 | 2.3 |
| $ZrO_2$ (75) | 35.2% | 9.2 | 75.0 |
| $TiO_2$ (1) | 4.3% | 67.9 | 1.0 |
| $TiO_2$ (51) | 80.3% | 22.6 | 51.3 |
| $TiO_2$ (80) | 100.0% | 14.6 | 80.0 |
| $TiO_2$ (337) | 100.0% | 8.9 | 337.0 |

[a]The compositions of the cubic phase in $CeO_2$, tetragonal phase in $ZrO_2$, and anatase phase in the $TiO_2$ samples

[b]The primary crystallite size was calculated for cubic $CeO_2$, tetragonal $ZrO_2$, and anatase $TiO_2$

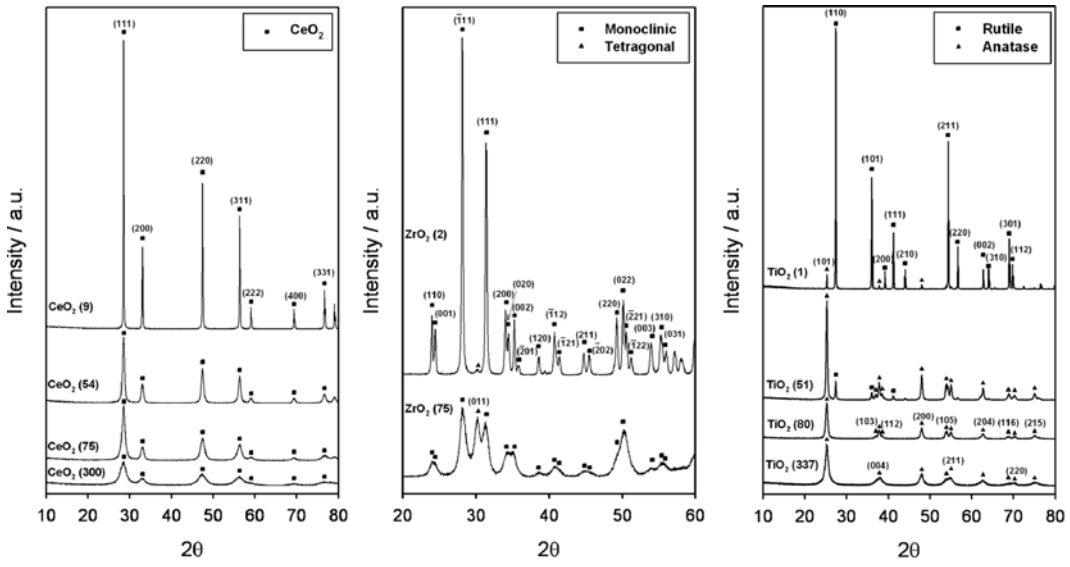


**Fig. 1. XRD patterns of $CeO_2$, $ZrO_2$, and $TiO_2$ used as supports.**

reactors were generally loaded with 0.10 g of the sample, and the catalysts were pretreated by reduction in $H_2$ at 673 K for 1 h, then cooled to room temperature. The CO chemisorption was carried out at 300 K in an He stream with a flow rate of 30 ml/min through the pulsed-chemisorption technique, in which 500 ml pulses of CO were utilized, after removing any residual hydrogen in the line by flowing He at 300 K for 1 h.

Temperature programmed reduction (TPR) was also conducted in an AutoChem 2910 unit (Micromeritics) equipped with a TCD to measure the $H_2$ consumption and an on-line mass spectrometer (QMS 200, Pfeiffer Vacuum) to detect any organic or inorganic species in the effluent stream during the TPR experiment. A water trap composed of blue silica gel removed moisture from the TPR effluent stream at 273 K before the TCD. Quartz U-tube reactors were generally loaded with 0.10 g of the sample, and the catalysts were pretreated by calcination in 20 vol% $O_2$ in $N_2$ at 773 K for 1 h, then cooled to room temperature. The TPR was performed using 10 vol% $H_2$/Ar with a flow rate of 30 ml/min in the temperature range from 313 K to 1,173 K at a heating rate of 10 K/min, while monitoring the TCD signals after removing any residual oxygen in the line by flowing He at 313 K for 1 h.

### 3. Catalytic Performance Tests

The catalytic activity was measured in a small fixed bed reactor with the catalyst that had been retained between 45 and 80 mesh sieves. For the screening tests, a standard gas consisting of 6.7 mol% CO, 6.7 mol% $CO_2$, and 33.2 mol% $H_2O$ balanced with $H_2$ was fed into the reactor, in which 0.10 g of catalyst without diluents was brought into contact with the reactant gas at a flow rate of 150 ml/min, at atmospheric pressure. The catalytic activity was measured with a ramping rate of 0.39 K/min.

The variation of the reaction rate with the time on stream was obtained at 583 K in the kinetically-controlled regime, which can be achieved by controlling the contact time.

The effluent from the reactor was passed through a condenser to remove the water vapor and analyzed by a gas chromatograph (HP5890A, Carbosphere column) to determine the CO conversion.

## RESULTS AND DISCUSSION

The X-ray diffraction patterns of the $CeO_2$, $ZrO_2$, and $TiO_2$ used as a support in this work are presented in Fig. 1. $CeO_2$ showed the typical XRD peaks representing a cubic cerianite phase (JCPDS No. 34-0394). $ZrO_2$ also exhibited distinct XRD peaks associated with monoclinic (JCPDS No. 37-1484) and tetragonal (JCPDS No. 50-1089) $ZrO_2$ crystallites. In the case of $TiO_2$, the tetragonal anatase (JCPDS No. 21-1272) and tetragonal rutile (JCPDS No. 21-1276) phases were observed. When compared with its surface area from Table 2, the XRD peak intensity of $CeO_2$ at $2\theta$=28.555° representing the (111) plane associated with cubic cerianite increased with decreasing surface area. The XRD peak intensity of $ZrO_2$ at $2\theta$=28.175° representing the plane associated with monoclinic $ZrO_2$ also increased with decreasing surface area. On the other hand, the XRD peak intensity of $ZrO_2$ at $2\theta$=30.269° representing the (011) plane associated with tetragonal $ZrO_2$ crystallites increased with increasing surface area. The XRD peak intensity of $TiO_2$ at $2\theta$=25.281°, which was indexed to the (101) plane of the tetragonal anatase phase increased with increasing surface area, showed a maximum value at $TiO_2$ (51), and then decreased as its specific surface area was further increased, while the XRD peak intensity of $TiO_2$ at $2\theta$=27.446°, which was indexed to the (110) plane of the tetragonal rutile phase decreased with increasing surface area. In the case of $TiO_2$ (80) and $TiO_2$ (337), no XRD peaks representing the rutile phase could be obtained.

Because the XRD peak intensity is closely related to the crystallinity, we conducted a further analysis of the XRD patterns to determine the ratio of each crystalline phase in $CeO_2$, $ZrO_2$, and $TiO_2$. As listed in Table 2, the ratio of tetragonal $ZrO_2$ and tetragonal anatase phase increased with increasing surface area, respectively. The primary crystalline sizes of $CeO_2$, $ZrO_2$, and $TiO_2$, calculated by XRD line broadening (Table 2), were inversely proportional to the surface area.

The effect of the support on the water-gas shift reaction was examined over the Pt catalysts supported on $CeO_2$, $ZrO_2$ and $TiO_2$, as

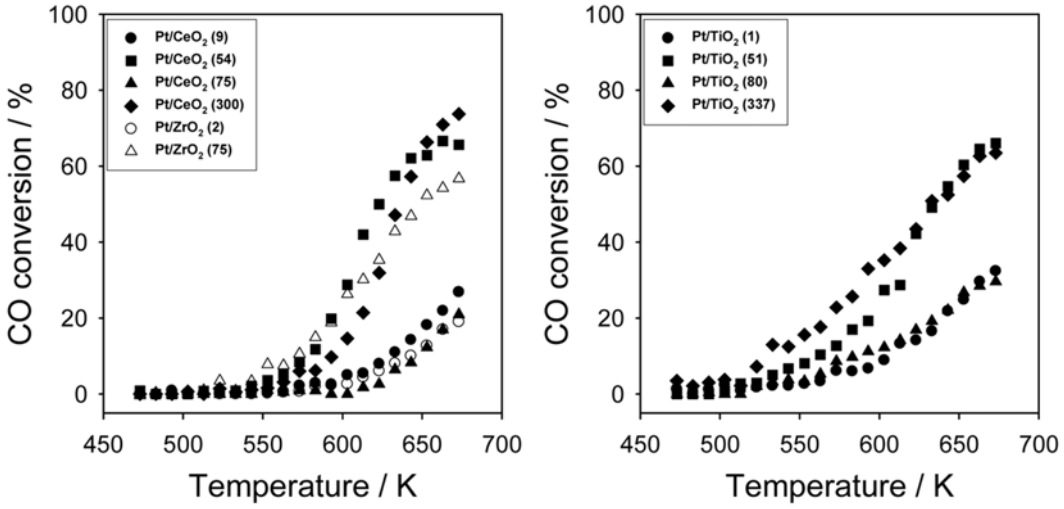


**Fig. 2. CO conversion over the Pt catalysts with increasing reaction temperatures. The feed composition was 6.7 mol% CO, 6.7 mol% $CO_2$, 33.2 mol% $H_2O$ in $H_2$. F/W=1,500 ml (STP)/min/$g_{cat.}$.**

shown in Fig. 2. The CO conversion at temperatures below 623 K decreased in the following order: $Pt/TiO_2$ (337)>$Pt/TiO_2$ (51)≈$Pt/CeO_2$ (54)>$Pt/ZrO_2$ (75)>$Pt/CeO_2$ (300)>>$Pt/TiO_2$ (80)>$Pt/TiO_2$ (1)>$Pt/CeO_2$ (9)>$Pt/ZrO_2$ (2)>$Pt/CeO_2$ (75). At temperatures above 623 K, the WGS activity increased noticeably with increasing reaction temperatures over $Pt/CeO_2$ (54), $Pt/CeO_2$ (300), and $Pt/TiO_2$ (51). Indeed, $Pt/CeO_2$ (54) and $Pt/CeO_2$ (300) showed the highest CO conversion at temperatures above 623 K among the supported Pt catalysts. In the case of the $TiO_2$-supported Pt catalysts, similar CO conversions were obtained over $Pt/TiO_2$ (51) and $Pt/TiO_2$ (337) at temperatures above 623 K. Under the same reaction conditions, the support itself did not show any detectable CO conversion at any reaction temperatures.

The effect of the support on the WGS activity was also investigated over the Pt-$CeO_x$ catalysts supported on $CeO_2$, $ZrO_2$ and $TiO_2$, as shown in Fig. 3. Compared with the supported Pt catalysts, all of the ceria-promoted Pt catalysts showed higher WGS activities at all reaction temperatures except for Pt-$CeO_x/TiO_2$ (337). The WGS activity at temperatures below 623 K decreased in the following order: Pt-$CeO_x/TiO_2$ (51)>Pt-$CeO_x/ZrO_2$ (75)>Pt-$CeO_x/TiO_2$ (80)>Pt-$CeO_x/CeO_2$ (300)≈Pt-$CeO_x/CeO_2$ (75)≈Pt-$CeO_x/CeO_2$ (54)≈Pt-$CeO_x/CeO_2$ (9)>Pt-$CeO_x/TiO_2$ (337)>Pt-$CeO_x/ZrO_2$ (2)>Pt-$CeO_x/TiO_2$ (1). Pt-$CeO_x/TiO_2$ (51) showed the highest WGS activity at all reaction temperatures.

The CO chemisorptions and reaction rates at 583 K for all of the supported Pt catalysts were measured and are listed in Table 3. The CO chemisorptions experiments were conducted to quantify the number of CO adsorption sites including Pt metal and reducible metal oxides.

In the case of the $CeO_2$-supported Pt catalysts, the Pt dispersion exceeded 100% except for $Pt/CeO_2$ (9) when the theoretical value was calculated based on the assumption that all of the Pt atom can chemisorb one CO molecule ($Pt_s$ : CO=1 : 1). No detectable chemisorbed CO was observed over the support itself. For the $Pt/CeO_2$

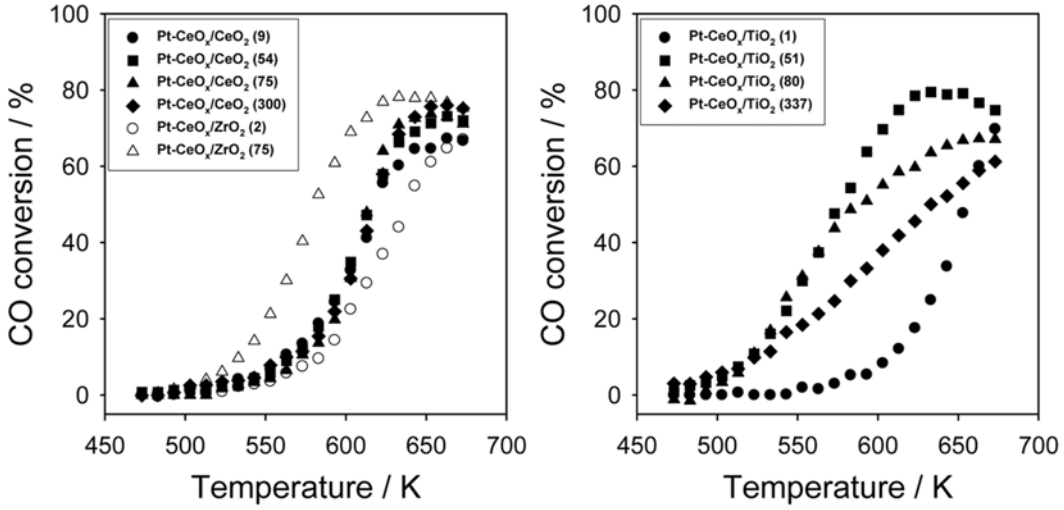


**Fig. 3. CO conversion over the Pt-$CeO_x$ catalysts (Ce/Pt=5) with increasing reaction temperatures. The feed composition was 6.7 mol% CO, 6.7 mol% $CO_2$, 33.2 mol% $H_2O$ in $H_2$. F/W=1,500 ml (STP)/min/$g_{cat.}$.**

catalyst, it was reported that the exceptionally large amount of chemisorbed CO might be due to the spillover process from Pt to the $CeO_2$ surface [26]. Another explanation is that the CO molecules react with $O^{2-}$ on ceria to form four different species, linearly adsorbed CO, unidentate carbonate, bidentate carbonate, and inorganic carboxylate species, as supported in FT-IR studies [27]. In our previous work on ceria-promoted Pt catalysts, we suggested that CO could be chemisorbed on Pt metal and reduced ceria near Pt metal, not on isolated reduced ceria on the support [20]. In the present work, the amount of chemisorbed CO generally increased with increasing surface area of the support except for Pt/$CeO_2$ (75) and Pt/$TiO_2$ (80). The exceptionally low amount of chemisorbed CO over Pt/$CeO_2$ (75) might be due to the presence of $Na^+$ impurity in the catalyst because $CeO_2$ (75) was prepared by the precipitation method with NaOH as a precipitation agent. The content of $Na^+$ was determined to be 0.05 wt% by ICP analysis. The adverse effect of $Na^+$ on the amount of chemisorbed CO was reported for Pt/Na/$CeO_2$ [7], Pt/Na/$TiO_2$ [18], and Pt-Na/$TiO_2$ [21]. It was reported that the addition of $Na^+$ to a support including Pt resulted in the weakening of the formate C-H bond on the Pt surface [7], the weakening of the Pt-H bond strength [18], and strengthening of the Pt-CO bond strength [18], and that the WGS activity was critically influenced by the amount of $Na^+$ [18,21].

In the case of Pt/$TiO_2$ (80), the crystal structure of $TiO_2$ might affect the amount of chemisorbed CO. A relatively poor dispersion of Pt can be achieved over anatase, as confirmed by the fact that a slightly larger amount of chemisorbed CO was achieved over Pt/$TiO_2$ (337) than over Pt/$TiO_2$ (51) although the former has a much larger specific surface area than the latter. Iida et al. reported that a rutile $TiO_2$-supported Pt catalyst had a higher Pt dispersion, CO conversion, and turnover frequency than an anatase $TiO_2$-supported Pt catalyst [16].

The results presented in Table 3 also indicate that the reaction rate at 583 K increased with increasing amount of chemisorbed CO, when the chemical composition of the support was kept the same except for the $CeO_2$-supported Pt catalysts. The reaction rate based on the number of moles of Pt at 583 K also showed similar results. The normalized reaction rates at 583 K, which were obtained by dividing the reaction rate by the amount of chemisorbed CO to compare the reaction rate per active site, are summarized in Table 3. Note that the normalized reaction rates are in the same order for the Pt catalysts supported on the metal oxides as long as the chemical composition of the support is the same. The only exception to this is Pt/$CeO_2$ (75), which might be due to the presence of $Na^+$ impurity as discussed in the CO chemisorptions data. In a previous work, we reported that reducible metal oxides can be considered to be better supports than irreducible metal oxides based on the normalized reaction rates [20]. The normalized reaction rate at 583 K decreased in the following order: Pt/$TiO_2$>>Pt/$ZrO_2$>Pt/$CeO_2$. Therefore, it is clear that the nature of the support affects the WGS activity. Pt/$TiO_2$ (337) showed the highest normalized reaction rate among the tested supported Pt catalysts.

The amount of chemisorbed CO was also measured for the supported Pt-$CeO_x$ catalysts and the results are listed in Table 4. Pt-$CeO_x$/$CeO_2$ (54), Pt-$CeO_x$/$CeO_2$ (75), Pt-$CeO_x$/$CeO_2$ (300), and Pt-$CeO_x$/$TiO_2$ (51) appeared to chemisorb larger amounts of CO than the theoretical value obtained based on the assumption that CO can be chemisorbed linearly on Pt atom. The $CeO_2$- and $ZrO_2$-supported Pt-$CeO_x$ catalysts showed the lower CO/Pt ratio than the corresponding supported Pt-only catalysts. On the other hand, the $TiO_2$-supported Pt-$CeO_x$ catalysts exhibited the larger amount of chemisorbed CO than the $TiO_2$-supported Pt-only catalysts. The most active catalyst, Pt-$CeO_x$/$TiO_2$ (51), can chemisorb the largest amount of CO, which can be interpreted to mean that the most intimate contact can be made between Pt and ceria for this catalyst. Compared with the $CeO_2$- and $ZrO_2$-supported Pt catalysts, a further increase in the reaction rate based on the number of moles of Pt and the normalized reaction rate was observed over the supported ceria-promoted catalysts.

Since the WGS activity is closely related to the interactions between Pt and the support (Fig. 2), $H_2$-TPR was carried out to probe the reducibility of the Pt catalysts, as shown in Fig. 4. The anchored metal such as Pt on the support can promote the reducibility of the surface metal oxides on the support. The TPR peak position and its intensity are closely related to the reducibility and amount of reducible species on the catalyst, respectively. These data can reveal the degree of interaction between Pt and the support on the catalyst. Platinum species, including $Pt_xO$ (surface platinum oxide), PtO, and $PtO_2$, could be reduced at low temperatures (<523 K) although the reducibility of platinum oxides is known to be dependent on their

**Table 3. Chemisorption data and reaction rates at 583 K for the supported Pt catalysts**

| Catalysts | CO chemisorption | | Reaction rate at 583 K ($\mu mol_{CO} \cdot g_{cat.}^{-1} \cdot s^{-1}$) | Reaction rate at 583 K ($mol_{CO} \cdot mol_{Pt}^{-1} \cdot s^{-1}$) | Normalized reaction rate at 583 K[a] ($s^{-1}$) |
|---|---|---|---|---|---|
| | CO uptake ($\mu mol/g_{cat.}$) | CO/Pt (%) | | | |
| Pt/$CeO_2$ (9) | 9.0 | 25.8 | 2.02 | 0.06 | 0.22 |
| Pt/$CeO_2$ (54) | 52.8 | 190.7 | 16.96 | 0.61 | 0.32 |
| Pt/$CeO_2$ (75) | 20.1 | 112.3 | 0.12 | 0.01 | 0.01 |
| Pt/$CeO_2$ (300) | 70.8 | 194.5 | 7.02 | 0.19 | 0.10 |
| Pt/$ZrO_2$ (2) | 5.7 | 21.0 | 1.63 | 0.06 | 0.29 |
| Pt/$ZrO_2$ (75) | 32.7 | 95.2 | 12.78 | 0.37 | 0.39 |
| Pt/$TiO_2$ (1) | 5.2 | 10.6 | 5.46 | 0.11 | 1.05 |
| Pt/$TiO_2$ (51) | 11.5 | 26.1 | 16.88 | 0.38 | 1.47 |
| Pt/$TiO_2$ (80) | 6.6 | 17.4 | 8.96 | 0.24 | 1.36 |
| Pt/$TiO_2$ (337) | 12.6 | 24.3 | 19.92 | 0.38 | 1.58 |

[a]The normalized reaction rate was calculated by dividing the reaction rate by the amount of chemisorbed CO based on the CO chemisorption

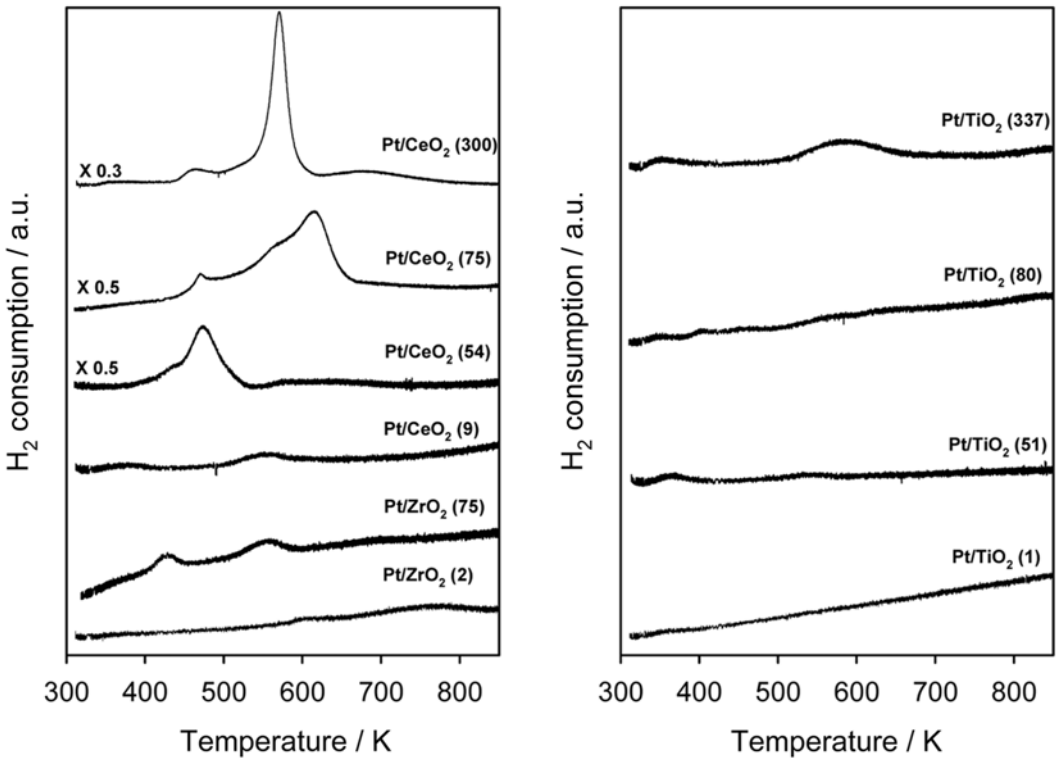


**Fig. 4. Temperature programmed reduction (TPR) patterns of the supported Pt catalysts calcined in air at 773 K.**

degree of crystallinity [17]. It was also reported that PtO interacting weakly with the support could be reduced at below room temperature [24,25]. According to the $H_2$-TPR results obtained over the Pt catalysts, due to the reduction of isolated platinum oxides, the reduction of surface platinum oxides interacting with the support, and the reduction of the surface oxides of the support, could be obtained with increasing temperature.

Two weak TPR peaks can be found over $Pt/CeO_2$ (9) at 374 and 552 K. In the case of $Pt/CeO_2$ (54), a strong peak was obtained at 474 K with a shoulder at 436 K, and a broad peak was also obtained at 623 K. For $Pt/CeO_2$ (75), two distinct separate peaks were found at 470 and 615 K with a shoulder at 568 K. On the other hand, four distinct peaks were obtained over $Pt/CeO_2$ (300) with maxima at 358, 463, 571, and 677 K. For the $Pt/CeO_2$ catalysts, the TPR peak positions in the range 373 to 470 K can be attributed to the reduction of surface platinum oxides interacting with the support. $Pt/CeO_2$ (54), the most active catalyst among the ceria-supported Pt catalysts, showed the strongest TPR peak especially at low temperatures, which implies that close intimate contact between Pt and the surface ceria can be made over this catalyst. The TPR peak positions in the range 474 to 615 K can be ascribed to the reduction of the ceria surface shell [7].

Two weak peaks were found over $Pt/ZrO_2$ (2) at 596 and 769 K, respectively. In the case of $Pt/ZrO_2$ (75), three distinct peaks were obtained at 430, 553, and 700 K, respectively. No distinguishable TPR peak in the range *ca.* 430 K, assigned to the reduction of the surface platinum oxides, was observed for $Pt/ZrO_2$ (2). The TPR peak position in the range 553 to 596 K, which is generally ascribed to the reduction of the zirconia surface shell [10], decreased with increasing surface area of the support. It is worth noting that the close intimate contact between Pt and the surface oxides of the support can be found over the more active $ZrO_2$-supported Pt catalyst, which is similar with the case of the ceria-supported Pt catalysts.

For $Pt/TiO_2$ (1), a weak peak was obtained at 362 K. For $Pt/TiO_2$ (51), two TPR peaks can be found at 366 and 542 K, respectively. Five distinct peaks can also be found over $Pt/TiO_2$ (80) at 349, 404, 464, 564, and 643 K. In the case of $Pt/TiO_2$ (337), two distinct separate peaks were observed at 351 and 583 K. The TPR peak positions over the $Pt/TiO_2$ catalysts in the range 349 to 369 K can be assigned to the reduction of surface platinum oxides interacting with the support. TPR peaks in the range 542 to 583 K, which were ascribed to the partial reduction of $TiO_2$ [17], were observed in the case of $Pt/TiO_2$ (51) and $Pt/TiO_2$ (337), respectively. The close intimate contact between Pt and surface oxides of the support was found over the more active $TiO_2$-supported Pt catalyst, which is similar to the ceria- and $ZrO_2$-supported Pt catalysts.

Based on the TPR data, we can say that new active sites are formed, originating from the intimate contact between the Pt species and the support. This is thought to be closely related to the increment of the WGS activity. The supported Pt catalyst which had the strongest TPR peak with a maximum at low temperatures, representing the intimate contact between $PtO_x$ and the support, showed the highest WGS activity.

To probe the reducibility of the supported ceria-promoted catalysts, TPR with $H_2$ was also conducted, as shown in Fig. 5. The TPR peaks of the supported Pt-$CeO_x$ catalyst can be divided into two parts for each sample. The low-temperature TPR (LTR) peak, which can be observed from 313 to 513 K, is due to the reduction of ceria near Pt metal and the high-temperature TPR (HTR) peak, which can be obtained above 473 K, is caused by the reduction of iso-

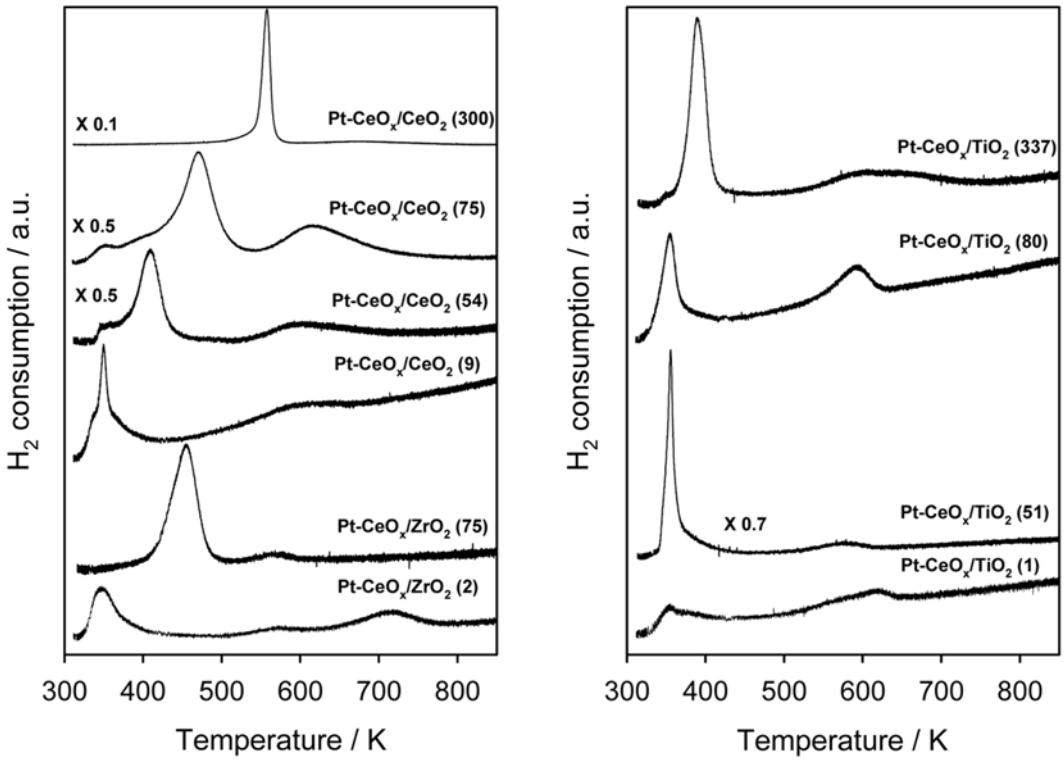


**Fig. 5. Temperature programmed reduction (TPR) patterns of the supported Pt-$CeO_x$ catalysts (Ce/Pt=5) calcined in air at 773 K.**

lated ceria on the catalyst [23]. The reduction temperature can be affected by various factors such as the degree of interaction between Pt and ceria, the crystalline size of ceria and the degree of interaction between ceria and the support. In the case of the TPR data for the support itself and the supported ceria, no TPR peaks were obtained in the low-temperature region. On the other hand, several TPR peaks were obtained over the supported ceria-promoted Pt catalyst. It is well known that the presence of noble metals such as Pt, Pd, and Rh significantly enhances the oxygen storage capacity (OSC) of $CeO_2$ anchored on a support [23]. The position of the TPR peak and its intensity are closely related to the reducibility and amount of reducible species on the catalyst, respectively.

Pt-$CeO_x$/$CeO_2$ (9) has two distinct separate TPR peaks at 349 K with a shoulder at 338 and 601 K. Three separate peaks can also be found over Pt-$CeO_x$/$CeO_2$ (54) at 345, 409, and 602 K. In the case of Pt-$CeO_x$/$CeO_2$ (75), three distinct separate peaks were obtained at 351, 471, and 616 K. For Pt-$CeO_x$/$CeO_2$ (300), a strong peak was obtained at 557 K and a broad peak was also found at 675 K. A stronger TPR peak was found over the ceria-promoted Pt/$CeO_2$ catalysts at lower temperatures compared with the Pt/$CeO_2$ catalysts, which confirms that the much stronger interaction can be obtained over the ceria-promoted Pt/$CeO_2$ catalysts. As revealed in Tables 3 and 4, the ceria-promoted Pt/$CeO_2$ catalyst showed a much higher WGS activity than the corresponding Pt catalyst supported on $CeO_2$. This result strongly supports the conclusion that the intimate contact between Pt and ceria plays an important role in the

**Table 4. Chemisorption data and reaction rates at 583 K for supported Pt-$CeO_x$ catalysts**

| Catalysts | CO chemisorption | | Reaction rate at 583 K ($\mu mol_{CO} \cdot g_{cat.}^{-1} \cdot s^{-1}$) | Reaction rate at 583 K ($mol_{CO} \cdot mol_{Pt}^{-1} \cdot s^{-1}$) | Normalized reaction rate at 583 K[a] ($s^{-1}$) |
|---|---|---|---|---|---|
| | CO uptake ($\mu mol/g_{cat.}$) | CO/Pt (%) | | | |
| Pt-$CeO_x$/$CeO_2$ (9) | 11.4 | 24.4 | 8.35 | 0.18 | 0.73 |
| Pt-$CeO_x$/$CeO_2$ (54) | 36.8 | 101.0 | 22.60 | 0.62 | 0.61 |
| Pt-$CeO_x$/$CeO_2$ (75) | 46.9 | 107.7 | 11.46 | 0.26 | 0.24 |
| Pt-$CeO_x$/$CeO_2$ (300) | 50.0 | 125.0 | 11.58 | 0.29 | 0.23 |
| Pt-$CeO_x$/$ZrO_2$ (2) | 6.5 | 17.0 | 8.54 | 0.22 | 1.31 |
| Pt-$CeO_x$/$ZrO_2$ (75) | 34.7 | 80.7 | 37.71 | 0.88 | 1.09 |
| Pt-$CeO_x$/$TiO_2$ (1) | 16.5 | 37.8 | 10.12 | 0.23 | 0.61 |
| Pt-$CeO_x$/$TiO_2$ (51) | 50.0 | 112.1 | 48.43 | 1.09 | 0.97 |
| Pt-$CeO_x$/$TiO_2$ (80) | 22.0 | 50.4 | 37.40 | 0.86 | 1.70 |
| Pt-$CeO_x$/$TiO_2$ (337) | 30.4 | 64.5 | 13.80 | 0.29 | 0.45 |

[a]The normalized reaction rate was calculated by dividing the reaction rate by the amount of chemisorbed CO based on the CO chemisorption

WGS reaction.

For Pt-$CeO_x$/$ZrO_2$ (2), three distinct separate peaks were obtained at 347, 573, and 716 K. A strong peak was obtained over Pt-$CeO_x$/$ZrO_2$ (75) at 455 K and a weak peak was also found at 568 K. It is also worth noting that a stronger TPR peak was found over the ceria-promoted Pt/$ZrO_2$ catalysts compared with the Pt/$ZrO_2$ catalysts, which supports the hypothesis that a much stronger interaction can be achieved over the ceria-promoted Pt/$ZrO_2$ catalysts. As revealed in Tables 3 and 4, the ceria-promoted Pt/$ZrO_2$ catalyst showed much higher WGS activity than the corresponding Pt catalyst supported on $ZrO_2$. This result strongly confirms that the intimate contact between Pt and ceria plays an important role in the WGS reaction.

Two broad separate peaks were obtained over Pt-$CeO_x$/$TiO_2$ (1) at 356 and 618 K. For Pt-$CeO_x$/$TiO_2$ (51), a strong peak was obtained at 356 K and a broad peak was also found at 576 K. In the case of Pt-$CeO_2$/$TiO_2$ (80), two distinct separate peaks were found at 354 and 592 K. Two distinct separate peaks were obtained over Pt-$CeO_x$/$TiO_2$ (337) at 389 K with a shoulder at 350 and 608 K. A stronger TPR peak was found over the ceria-promoted Pt/$TiO_2$ catalysts compared with the Pt/$TiO_2$ catalysts, which supports the finding that a much stronger interaction can be obtained over the ceria-promoted Pt/$TiO_2$ catalysts. As shown in Tables 3 and 4, all of the ceria-promoted Pt/$TiO_2$ catalyst except for Pt-$CeO_x$/$TiO_2$ (337) showed much higher WGS activity than the corresponding Pt catalyst supported on $TiO_2$. In the case of Pt-$CeO_x$/$TiO_2$ (337), the WGS activity slightly decreased even though a stronger low-temperature TPR peak was found over this catalyst compared with Pt/$TiO_2$ (337). Further work seems to be required to resolve this discrepancy. One possible reason might be the drastic change in the surface area of $TiO_2$ during the preparation of the catalyst. The surface area decreased to one third of its initial value, which might cause a severe change in the texture properties of the final catalyst, resulting in a decrease in the WGS activity.

The amount of $H_2$ consumed in the LTR region can reveal the

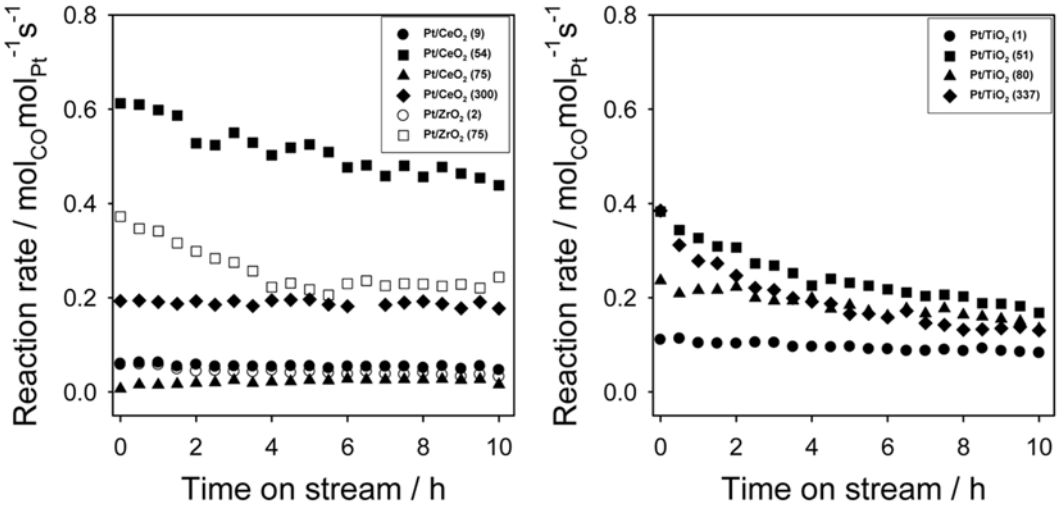


**Fig. 6. Variation of the reaction rates at 583 K for the supported Pt catalysts with the time on stream. The feed composition was 6.7 mol% CO, 6.7 mol% $CO_2$, 33.2 mol% $H_2O$ in $H_2$.**

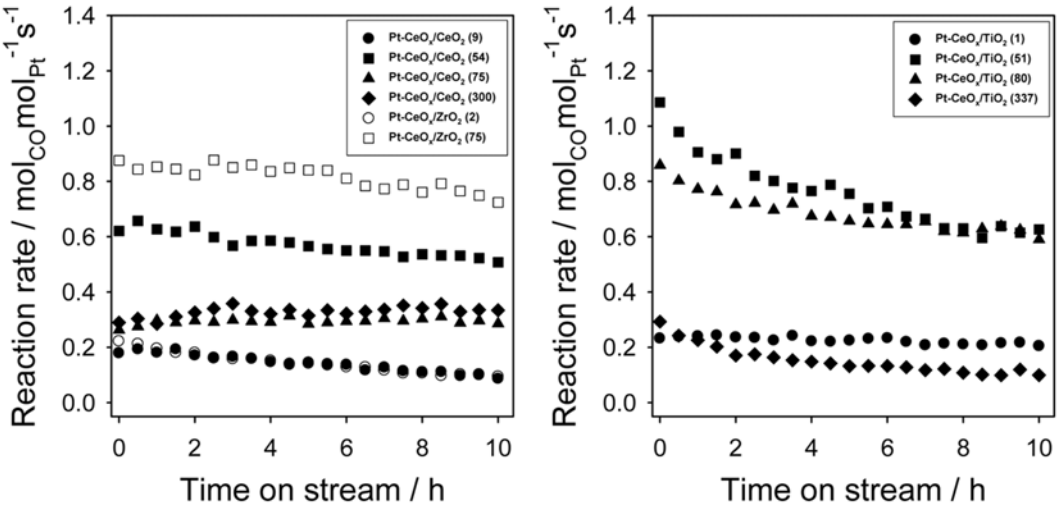


**Fig. 7. Variation of the reaction rates at 583 K for the supported Pt-$CeO_x$ catalysts with the time on stream. The feed composition was 6.7 mol% CO, 6.7 mol% $CO_2$, 33.2 mol% $H_2O$ in $H_2$.**

degree of interaction between Pt and ceria on the catalyst. The LTR peak position generally shifted to a lower temperature with increasing reaction rate on the supported Pt-$CeO_x$ catalysts. This implies that the close contact between Pt and ceria on the support is closely related to the WGS activity over the supported Pt-$CeO_x$ catalysts. The most active catalyst, Pt-$CeO_x$/$TiO_2$ (51), showed the strongest LTR peak at low temperatures.

Besides the high initial catalytic activity, stable catalytic activity is highly necessary for WGS catalysts to be applied to commercial processes. Fig. 6 shows the variation of the WGS activity at 583 K with the time on stream over the supported Pt catalysts. Fig. 7 shows the variation of the WGS activity at 583 K with the time on stream over the supported Pt-$CeO_x$ catalysts. Pt-based catalysts can suffer from deactivation over the WGS stream, because of carbonate species poisoning [6,8], Pt sintering [19,20], the loss of active metal surface area [14], and support degradation such as "over"-reduction [15,19]. The catalytic stability at 583 K increased with increasing surface area of the supports for the $CeO_2$- and $ZrO_2$-supported Pt and Pt-$CeO_x$ catalysts. The stability of Pt-$CeO_x$/$CeO_2$ (9) and Pt-$CeO_x$/$ZrO_2$ (2) was poor. Pt-Ce/$TiO_2$ (51), which has the largest amount of surface active sites and the highest initial WGS activity, showed a gradual decrease in its WGS activity at 583 K, which may be due to the sintering of Pt and the weakening interaction between Pt and ceria, as revealed in our previous work [20].

Although Pt-$CeO_x$/$CeO_2$ (54) showed stable catalytic activity, it was reported that $CeO_2$-supported Pt catalyst suffered from severe deactivation during the start-up/shut-down test, in which cerium(III) hydroxycarbonate was formed [8,20]. Therefore, Pt-$CeO_x$/$ZrO_2$ (75) can be selected as the most promising catalyst, because it has a relatively high initial catalytic activity and stability.

## CONCLUSIONS

A comparison work was carried out for the water-gas shift (WGS) reaction over Pt and ceria-promoted Pt catalysts supported on $CeO_2$, $ZrO_2$, and $TiO_2$ under severe reaction conditions: 6.7 mol% CO, 6.7 mol% $CO_2$, and 33.2 mol% $H_2O$ in $H_2$. The WGS reaction rate increased with increasing amount of chemisorbed CO over Pt/$ZrO_2$, Pt/$TiO_2$, and Pt-$CeO_x$/$ZrO_2$. This proportional relationship was not observed over Pt/$CeO_2$, Pt-$CeO_x$/$CeO_2$, and Pt-$CeO_x$/$TiO_2$. For these catalysts in the absence of any impurities such as $Na^+$, the WGS activity increased with increasing surface area of the support, exhibited a maximum value, and then decreased as the surface area of the support was further increased. The adverse effect of $Na^+$ on the amount of chemisorbed CO and the WGS activity was confirmed over Pt/$CeO_2$. Pt-$CeO_x$/$TiO_2$ (51) showed the highest WGS activity among the tested supported Pt and Pt-$CeO_x$ catalysts. The close contact between Pt and the support or between Pt and $CeO_x$, as observed by $H_2$-TPR, is closely related to the WGS activity. The catalytic stability at 583 K improved with increasing surface area of the support over the $CeO_2$- and $ZrO_2$-supported Pt and Pt-$CeO_x$ catalysts.

## ACKNOWLEDGEMENTS

This work was supported by the Next Generation Military Battery Research Center program of the Defense Acquisition Program Administration and Agency for Defense Development.

## REFERENCES

1. M. I. Temkin, *Adv. Catal.*, **28**, 173 (1979).
2. D. S. Newsome, *Catal. Rev. Sci. Eng.*, **21**, 275 (1980).
3. O. Ilinich, W. Ruettinger, X. S. Liu and R. Ferrauto, *J. Catal.*, **247**, 112 (2007).
4. T. Giroux, S. Hwang, Y. Liu, W. Ruettinger and L. Shore, *Appl. Catal. B: Environ.*, **56**, 95 (2005).
5. P. Panagiotopoulou and D. I. Kondarides, *Catal. Today*, **112**, 49 (2006).
6. X. H. Liu, W. Ruettinger, X. Xu and R. Farrauto, *Appl. Catal. B: Environ.*, **56**, 69 (2005).
7. H. N. Evin, G. Jacobs, J. Ruiz-Martinez, G. A. Thomas and B. H. Davis, *Catal. Lett.*, **120**, 166 (2008).
8. W. L. Deng and M. Flytzani-Stephanopoulos, *Angew. Chem.*, **118**, 2343 (2006).
9. D. Tibiletti, F. C. Meunier, A. Goguet, D. Reid, R. Burch, M. Boaro, M. Vicario and A. Trovarelli, *J. Catal.*, **244**, 183 (2006).
10. S. Ricote, G. Jacobs, M. Milling, Y. Ji, P. M. Patterson, B. H. Davis, *Appl. Catal. A: Gen.*, **303**, 35 (2006).
11. H. C. Lee, D. H. Lee, O. Y. Lim, S. H. Kim, Y. T. Kim, E. Y. Ko and E. D. Park, *Stud. Surf. Sci. Catal.*, **167**, 201 (2007).
12. R. Radhakrishnan, R. R. Willigan, Z. Dardas and T. H. Vanderspurt, *AIChE J.*, **52**, 1888 (2006).
13. M. Laniecki and M. Ignacik, *Catal. Today*, **116**, 400 (2006).
14. X. Wang, R. J. Gorte and J. P. Wagner, *J. Catal.*, **212**, 225 (2002).
15. J. M. Zalc, V. Sokolovskii and D. G. Löffler, *J. Catal.*, **206**, 169 (2002).
16. H. Iida and A. Igarashi, *Appl. Catal. A: Gen.*, **298**, 152 (2006).
17. P. Panagiotopoulou, A. Christodoulakis, D. I. Kondarides and S. Boghosian, *J. Catal.*, **240**, 114 (2006).
18. P. Panagiotopoulou and D. I. Kondarides, *J. Catal.*, **267**, 57 (2009).
19. K. G. Azzam, I. V. Babich, K. Seshan and L. Lefferts, *Appl. Catal. A: Gen.*, **338**, 66 (2008).
20. Y. T. Kim, E. D. Park, H. C. Lee, D. Lee and K. H. Lee, *Appl. Catal. B: Environ.*, **90**, 45 (2009).
21. X. Zhu, T. Hoang, L. L. Lobban and R. G. Mallinson, *Catal. Lett.*, **129**, 135 (2009).
22. I. D. González, R. M. Navarro, W. Wen, N. Marinkovic, J. A. Rodriguéz, F. Rosa and J. L. G. Fierro, *Catal. Today*, **149**, 372 (2010).
23. H. C. Yao and Y. F. Yu Yao, *J. Catal.*, **86**, 254 (1984).
24. C.-P. Hwang and C.-T. Yeh, *J. Mol. Catal. A: Chem.*, **112**, 295 (1996).
25. R. W. McCabe, C. Wong and H. S. Woo, *J. Catal.*, **114**, 354 (1988).
26. A. Holmgren and B. Andersson, *J. Catal.*, **178**, 14 (1998).
27. C. Li, Y. Sakata, T. Arai, K. Domen, K. I. Maruya and T. Onishi, *J. Chem. Soc. Faraday Trans.1*, **85**, 929 (1989).
28. R. Srinivasan, M. B. Harris, S. F. Simpson and B. H. Davis, *J. Mater. Res.*, **3**, 787 (1988).
29. R. A. Spurr and H. Myers, *Anal. Chem.*, **59**, 761 (1957).